Chattering Free High Order Sliding Mode Observer for Estimation of Liquid Water Fraction in a Proton Exchange Membrane Fuel Cell

Julio Luna[1,*], *Member, IEEE* and Ramon Costa-Castelló[2], *Senior Member, IEEE*

Abstract— In this work, a methodology for the estimation of the liquid fraction of a proton exchange membrane fuel cell (PEMFC) is developed. Specifically, a model-based chattering-free high order sliding mode (CHOSM) observer is designed for the estimation of two dynamic states: the PEMFC temperature and the liquid water saturation. The observation strategy is discussed in a simulation environment using the common ARTEMIS driving cycle (CADC) as a case study.

I. INTRODUCTION

As energy consumption increases, society, industry and governments have become aware of the necessity to deploy new sustainable energy systems that can cut down the problems associated with the use of fossil fuels and other non-renewable energies. Making use of these energy sources generates carbon emissions and is not sustainable on a long-term time horizon. Accomplishing this technological and social shift requires high amounts of investments and research efforts addressed to alternative and clean energy sources. Moreover, the problems of storage and transportability have to be addressed when studying sustainable energy generation solutions. Researchers [1], [2] have pointed out that it is necessary for future energy systems to make use of energy carriers that can be produced from renewable power sources.

Research studies [3], [4] have concluded that energy generation systems that use hydrogen can be a potential solution to satisfy the present and future energy demands without additional carbon emissions. Hydrogen as an energy vector has significant advantages compared to other power carriers and its use can aid to reduce gas emissions and to diversify the energy generation market [5]. This is mainly because hydrogen has the possibility to be produced from renewable primary energy sources (i.e. solar and eolic). Moreover, hydrogen can be burned directly in gas turbines to obtain electricity, producing only water and heat as by-products. It also may be used to feed a fuel cell. Long-term storage is also a feature of hydrogen, making it perfect for long distance transport and mobile applications.

Proton exchange membrane fuel cells (PEMFCs), which use hydrogen as fuel and have high power densities while operating at low temperatures, are gaining increasing attention as clean and efficient energy conversion devices for a broad range of applications: automotive, stationary combined heat and power (CHP) and portable systems. Researchers from all over the world are dedicating a great effort to improve efficiency, reduce degradation and decrease the production costs of PEMFC technology. In order to optimise their performance, PEMFC systems require active control and therefore, in-depth knowledge of the system dynamics, which include multi-physics phenomena such as fluid mechanics, thermal dynamics and chemical kinetics.

Efficiency and degradation of PEMFCs are directly related with the internal operating conditions. In the automatic control field, new observation [6], diagnosis [7] and control [8] solutions are being developed to improve the operating conditions of PEMFC based systems. The system temperature, gas species concentrations, current density and water content are some of the variables that affect the performance of the system. Additionally, the remaining useful life of a PEMFC is drastically reduced when the system is subjected to sudden and unexpected load changes that can trigger reactant starvation scenarios.

Quantifying degradation in PEMFCs is a challenging task. One of the approaches proposed in the literature [9] is to model the electrochemically effective area of the cathode. This area is a measure of the total active platinum (Pt) available in the cathode catalyst layer (CCL). The amount of active Pt particles depends, among others, on the Pt loading of the CCL during the manufacturing process and the hydration state of the cathode. The hydration state is the only variable that can be actively controlled by modifying the temperature of the stack and the inlet cathode relative humidity (RH). However, determining its value while the system is being operated is not possible with the current sensor technology. In this sense, advanced models and estimation procedures can help to determine the hydration state of the cathode and deploy active control solutions that can manipulate this variable.

Modelling plays a key role in the research areas of control and health monitoring of PEMFCs. In fact, in order to develop and deploy control strategies that aid to improve efficiency and enhance the durability of PEMFC systems, mathematical models are necessary. Effects of the operating conditions on the fuel cell performance have been studied by several authors with different experimental approaches. However, while experimental analysis gives back reliable information about the performance of the system, it can be exceedingly expensive and inaccurate (i.e. not being able to represent the internal dynamics of the fuel cell). Mathematical models aid to reduce experimentation costs and they can be used to develop control and observation techniques that study aspects of the fuel cell that can not be

[1]Julio Luna is with the Electrical Engineering Department, Chalmers University of Technology, Hörsalsvägen 11, SE-412 96, Göteborg, Sweden

[2]Ramon Costa-Castelló is with the Institut de Robòtica i Informàtica Industrial, Universitat Politècnica de Catalunya, Carrer Llorens i Artigàs 4-6, 08028, Barcelona, Spain

*Corresponding author: `julio.luna@chalmers.se`

analysed conveniently through experimental measurements.

Estimation of internal states and performance variables in PEMFC systems is a topic directly related with the implementation of advanced control techniques to improve efficiency and durability. While a certain amount of measurements are feasible using the existing sensor technology, there are parts of the system that are inaccessible because of its structure. Distributed parameter models combined with model-based state estimation techniques is a novel solution to study the internal conditions in PEMFC, with the possibility of using this information in a control strategy [10]. Additionally, the use of mathematical observation tools is directly related with the reduction of the number of sensors and their associated cost [11], hence state observation tools can aid in the reduction of the overall cost of PEMFC systems.

The main contribution of this work relies on the development of a nonlinear observer that uses quasi-continuous sliding mode techniques to estimate the liquid water fraction inside a PEMFC. A dynamic model of an open cathode PEMFC is used to design the observer.

The paper is organised as follows. In Section II, the general system description is introduced. In Section III the simulation model of the open cathode PEMFC is presented. The observation problem and the liquid water fraction observer are developed in Section IV. Simulation results of the proposed observer for a common ARTEMIS driving cycle (CADC) case study are presented and analysed in detail in Section V. Finally, Section VI summarises the results of this paper and proposes research lines for future work.

II. SYSTEM DESCRIPTION

In this study, the commercial PEMFC stack H-100 developed by *Horizon Fuel Cells Technologies* is analysed and modelled in Section III. This stack is composed of 20 cells and has a rated power of 100 W. It has an open-cathode and does not require reactant gas humidification. It is air cooled and has an active area of 22.5 cm^2.

Figure 1 shows a schematic diagram of the fuel cell system installed in the laboratory test station. The fan is powered by a 12 V external power source. A controller sets the rotational speed of the fan by adjusting the PWM duty cycle. The air speed is measured using a high precision airflow sensor *E75 E + E Elektronik*. The anode inlet is fed with dry hydrogen. A manual pressure regulator keeps the pressure of the anode inlet constant at about 0.4 bar.

III. FUEL CELL MODEL

In a previous work [12], a dynamic second-order model has been developed for the system described in Section II. The model is defined by the following set of equations:

$$
\begin{aligned}
\dot{T}_{fc} &= K_1 \cdot I_{fc} V_{fc} + K_1 \cdot I_{fc}^2 \\
&\quad + (K_2 \cdot T_{amb} - K_2 \cdot T_{fc}) u_{air}, \quad (1) \\
\dot{s}_{fc} &= K_3 \cdot T_{fc} - K_4 \cdot f_p (T_{fc}) \cdot s_{fc} - f_d (s_{fc}), \quad (2) \\
V_{fc} &= K_5 \cdot T_{fc} \cdot f_a (T_{fc}, s_{fc}, I_{fc}). \quad (3)
\end{aligned}
$$

The dynamic states correspond to the fuel cell temperature (T_{fc}) and liquid water saturation (s_{fc}). The system has 3

inputs which are the fuel cell current (I_{fc}), the ambient temperature (T_{amb}) and the cathode inlet air velocity (u_{air}). The latter is often used as control action. The output of the system, V_{fc}, corresponds to the fuel cell stack voltage. Thus, the generated electrical power by the stack is defined by $P_{fc} = V_{fc} \cdot I_{fc}$.

The equations (1)-(3) are highly nonlinear, because of the involved complex expressions f_a, f_d and f_p composed by nonlinear components [12]. In addition, the control action is multiplied by K_i functions that depend on the dynamic states. Appendix A contains the expressions for all the parameters.

Equations (1)-(3) can be partially simplified by the following variable change:

$$
u_{air} \triangleq \frac{\nu}{K_2 T_{amb} - K_2 T_{fc}}, \quad (4)
$$

where ν corresponds to the heat extracted from the system. With this variable change, the system description results in

$$
\begin{aligned}
\dot{T}_{fc} &= K_1 \cdot I_{fc} \cdot V_{fc} + K_1 \cdot I_{fc}^2 + \nu, \quad (5) \\
\dot{s}_{fc} &= K_3 \cdot I_{fc} - K_4 \cdot f_p (T_{fc}) \cdot s_{fc} - f_d (s_{fc}), \quad (6) \\
V_{fc} &= K_5 \cdot T_{fc} \cdot f_a (T_{fc}, s_{fc}, I_{fc}). \quad (7)
\end{aligned}
$$

IV. HOSM OBSERVER

Following the nonlinear observer structure proposed by [13], the observer for Equations (5)-(7) is expressed as

$$
\begin{aligned}
\dot{\hat{x}}_1 &= K_1 I_{fc} - K_1' I_{fc} V_{fc} + \nu + g_1(\hat{\mathbf{x}}) u_1, \quad (8a) \\
\dot{\hat{x}}_2 &= K_3 I_{fc} - K_4 f_p(\hat{x}_1) \hat{x}_2 - f_d(\hat{x}_2) + g_2(\hat{\mathbf{x}}) u_2, \quad (8b) \\
\hat{y} &= h(\hat{\mathbf{x}}) = \hat{x}_1, \quad (8c)
\end{aligned}
$$

where $\hat{\mathbf{x}} \triangleq [\hat{x}_1, \hat{x}_2]$, $\hat{x}_1 \triangleq \hat{T}_{fc}$ and $\hat{x}_2 \triangleq \hat{s}_{fc}$. The observed output variable is the temperature of the fuel cell as denoted by Equation (8c). Functions g_1 and g_2 and the corrective terms u_1 and u_2 will be designed in order to reduce the estimation error to zero in a finite amount of time.

A. Observability analysis

In nonlinear systems, the study of the observability is related with the rank of a given observability matrix $\mathcal{O}$ [13]. In particular, the observability matrix is defined as

$$
\mathcal{O}(\mathbf{x}) = \frac{\partial}{\partial \mathbf{x}}
\begin{bmatrix}
h(\mathbf{x}) \\
L_{f(\mathbf{x})} h(\mathbf{x}) \\
\vdots \\
L_{f(\mathbf{x})}^{n-1} h(\mathbf{x})
\end{bmatrix}, \quad (9)
$$

where n is the number of states in $\mathbf{x}$ and $L_{f(\mathbf{x})} h(\mathbf{x})$ is the Lie derivative of the output vector h along the vector field $f(\mathbf{x}) \in \mathbb{R}^n$, defined as follows [14]:

$$
L_{f(\mathbf{x})} h(\mathbf{x}) = \frac{\partial h(\mathbf{x})}{\partial \mathbf{x}} f(\mathbf{x}). \quad (10)
$$

And the k-th Lie derivative:

$$
L_{f(\mathbf{x})}^k h(\mathbf{x}) = \frac{\partial \left(L_{f(\mathbf{x})}^{k-1} h(\mathbf{x}) \right)}{\partial \mathbf{x}} f(\mathbf{x}). \quad (11)
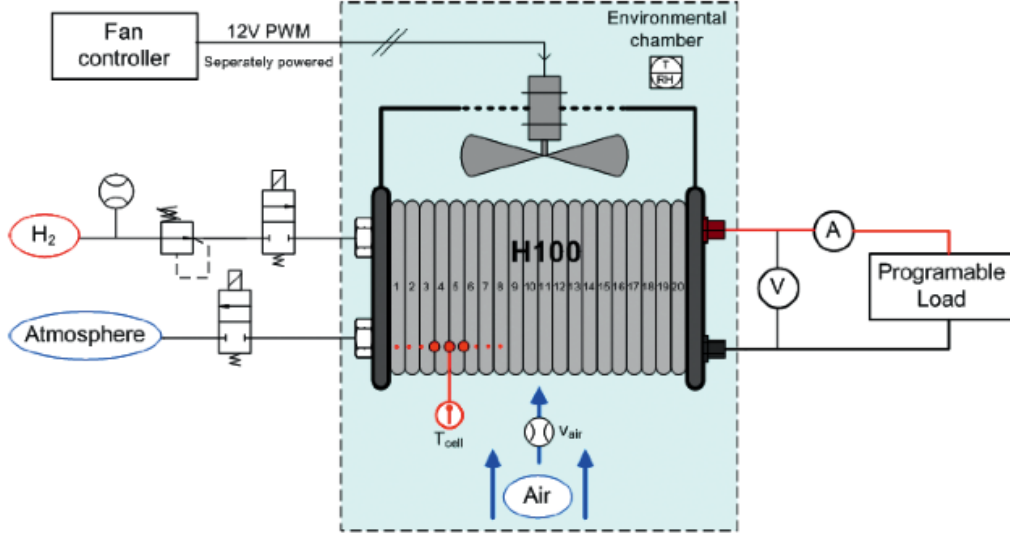$$

Fig. 1. Schematic of the fuel cell system H-100 installed in the laboratory test station

Using Equations (10) on Equation (8), the observability matrix is obtained:

$$\mathcal{O}(\hat{\mathbf{x}}) = \begin{bmatrix} 1 & 0 \\ \xi(\hat{\mathbf{x}}) & \gamma(\hat{\mathbf{x}}) \end{bmatrix}, \tag{12}$$

being ξ and γ nonlinear functions that depend on the states of the system.

As demonstrated by [13], to guarantee the observability of Equation (8), the rank of $\mathcal{O}$ has to be equal to n, being $n = 2$ in this work (two states). The rank of Equation (12) only depends on γ, which is defined as

$$\gamma(\hat{\mathbf{x}}) = -\frac{I_{fc}K_1' K_5 \hat{x}_1}{3s^{opt}\left(1 - \frac{s^{opt} - \hat{x}_2}{s^{opt}}\right)}, \tag{13}$$

being s^{opt} the optimal water content for the H-100 PEMFC, defined in Table I.

The condition that guarantees that $rank(\mathcal{O}) = 2$ is

$$\gamma(\hat{\mathbf{x}}) \neq 0. \tag{14}$$

Since K_1' and K_5 are constant, non-zero parameters (see Appendix A), the condition (14) holds if x_1, x_2 and I_{fc} are different from 0.

Once the observability is guaranteed, functions g_1 and g_2 in Equation (8) are obtained as follows [13]:

$$\mathbf{g}(\hat{\mathbf{x}}) = \begin{bmatrix} g_1(\hat{\mathbf{x}}) \\ g_2(\hat{\mathbf{x}}) \end{bmatrix} = \mathcal{O}(\hat{\mathbf{x}})^{-1} \begin{bmatrix} 0 & 1 \end{bmatrix}^T, \tag{15}$$

which results in $g_1(\hat{\mathbf{x}}) = 0$ and $g_2(\hat{\mathbf{x}}) = \frac{3I_{fc}\hat{x}_2}{K_1' K_5 \hat{x}_1}$.

Finally, considering g_1 and g_2, Equation (8) is expressed as

$$\dot{\hat{x}}_1 = K_1 I_{fc} - K_1' I_{fc} V_{fc} + \nu, \tag{16a}$$

$$\dot{\hat{x}}_2 = K_3 I_{fc} - K_4 f_p(\hat{x}_1)\hat{x}_2 - f_d(\hat{x}_2) + \frac{3I_{fc}\hat{x}_2}{K_1' K_5 \hat{x}_1}u_2, \tag{16b}$$

$$\hat{y} = \hat{x}_1. \tag{16c}$$

B. Correcting action design

Since the only state measurement is T_{fc}, the observation error e_y is expressed as the difference between the estimated output $\hat{y}$ of the observer and the measured vector y:

$$e_y = \hat{y} - y = \hat{x}_1 - x_1. \tag{17}$$

The sliding surface σ is chosen as follows:

$$\sigma = e_y. \tag{18}$$

And the sliding manifold ℓ for the sliding surface in Equation (18) is

$$\ell = \dot{\sigma} - k\sigma, \tag{19}$$

where k is a positive parameter.

To drive Equation (17) to zero in a finite amount of time, a second-order quasi-continuous correction input u_2 is implemented [15]:

$$u_2 = -\beta\left(\frac{\dot{\sigma} + |\sigma|^{1/2}sign(\sigma)}{|\dot{\sigma}| + |\sigma|^{1/2}}\right), \tag{20}$$

where β is the gain of the observer.

C. Chattering-free HOSM Observer

To solve the chattering problem in Equation (20), an adaptive $\hat{\beta}$ gain is proposed in this section.

Following the methodology proposed by [16], the derivative of the adaptive gain for the corrective input in Equation (20) is defined as

$$\dot{\hat{\beta}} = \begin{cases} \theta \left(-\rho\hat{\beta} + ||\sigma - \wp|| \right), & \text{if } \ell \neq 0, \\ 0, & \text{otherwise,} \end{cases} \quad (21)$$

being $\theta, \rho \in \mathbb{R}^+$ constants to be tuned. The variable $\wp$ represents a small positive number introduced to maintain $\hat{\beta}$ at the smallest possible value while preserving state estimation capabilities in the presence of uncertainties [16].

V. RESULTS

In this section, the observer developed in Section IV is tested by simulation using the driving cycle described in Section V-A. The CHOSM observer in Equation (16) uses the adaptive gain in Equation (21) with $\theta = 5$, $\rho = 10$ and $\wp = 1e^{-4}$. The initial state of the estimation is assumed to be $\hat{\mathbf{x}}(0) = [\hat{x}_1(0), \hat{x}_2(0)] = [298\ K, 0]$.

A. Case study

A CADC driving cycle [17] is used to test the observation strategy in a simulation framework. The CADC is a speed profile (see Figure 2) that represents urban and motorway driving scenarios to evaluate pollutant emissions and energy management strategies. In this work, the CADC motorway speed profile is used to test the power demand that the fuel cell has to deliver. Considering no hybridisation of the system, it is assumed that the fuel cell has to provide all of the demanded power. Because of this, the 20 cells of the laboratory H-100 have been substituted by 370 cells in the simulations, the same amount of cells present in the Toyota Mirai [18].

A virtual car model [19] is implemented to transform the speed profile to a power demand profile, assuming that a low level control system (not presented in this paper) allows the fuel cell to provide enough power to follow the speed profile. The required power profile is shown in Figure 3. It has to be noted that the auxiliary subsystems consume $400\ W$ when the car is stopped. Figure 4 shows the current and voltage of the PEMFC during the simulation profile. The current corresponds to one of the model inputs and the total stack voltage is one of the measured outputs.

B. Results and discussion

Figure 5(a) shows the evolution of the fuel cell temperature, T_{fc}, the HOSM observer estimation $\hat{T}_{fc}$ and the CHOSM observer estimation $\hat{T}_{fc,cf}$. Similarly, Figure 5(b) shows the dynamic response of the liquid water fraction s_{fc}, the HOSM estimation $\hat{s}$ and the CHOSM estimation response $\hat{s}_{cf}$. It has to be remarked again that s_{fc} can not be measured and its estimation is especially valuable for future control applications using the proposed observers.

As shown in Figure 5(a) and (b), the observation of both states (red dashed line for the HOSM observer and black
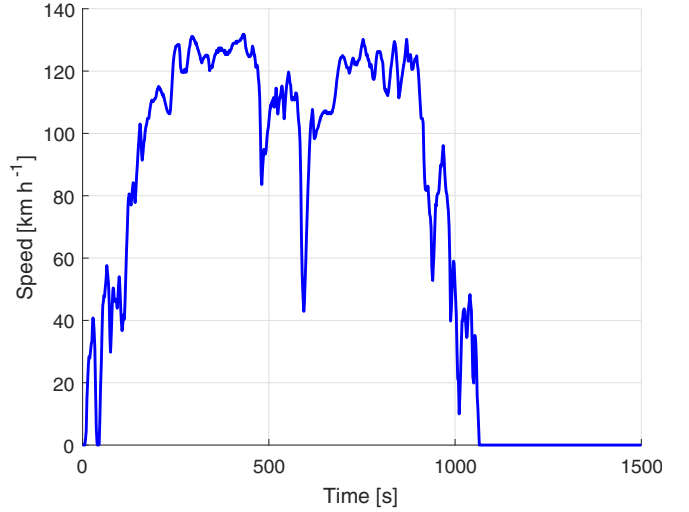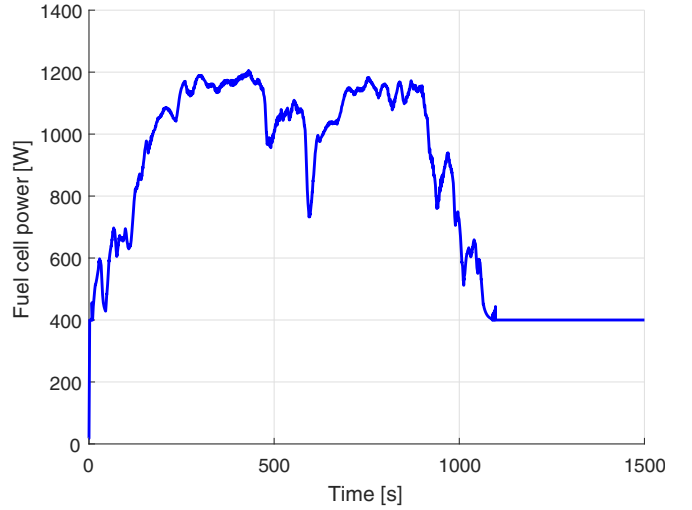

Fig. 2.   CADC motorway speed profile

Fig. 3.   Power profile needed to follow the CADC speed profile

dashed line for the CHOSM observer) is performed satisfactorily through all the simulation scenario. Specifically, Figure 5(a) shows how the CHOSM observer is slightly faster than the HOSM. In a similar way, the CHOSM observer performs faster for the estimation of s_{fc} in Figure 5(b). However, the overshooting before stabilisation is greater than in the HOSM case.

Figure 6 shows the corrective action for the HOSM and CHOSM observers (u_2 and $u_{2,cf}$ respectively). These corrective actions are used to drive the observation error in Equation (17) to zero in a finite amount of time. Both signals have an initial transitory response where $e_y \neq 0$. After a short period of time, u_2 starts commuting to guarantee that the state variables are kept on the sliding surface that makes that the estimated states are the same as the model states as shown in Figure 5. However, as it can be observed in the detail of Figure 6, there is a switching dynamic for the HOSM case. This switching, when implementing the observer in the real laboratory system, can create issues with the measuring
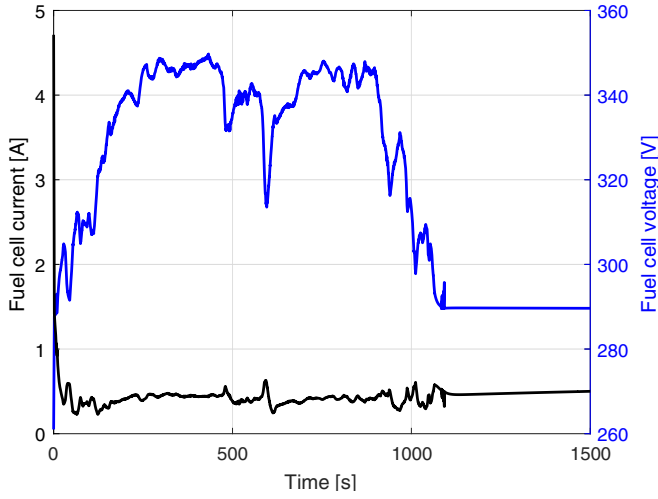
Fig. 4. Current and voltage profiles provided by the PEMFC during the CADC profile
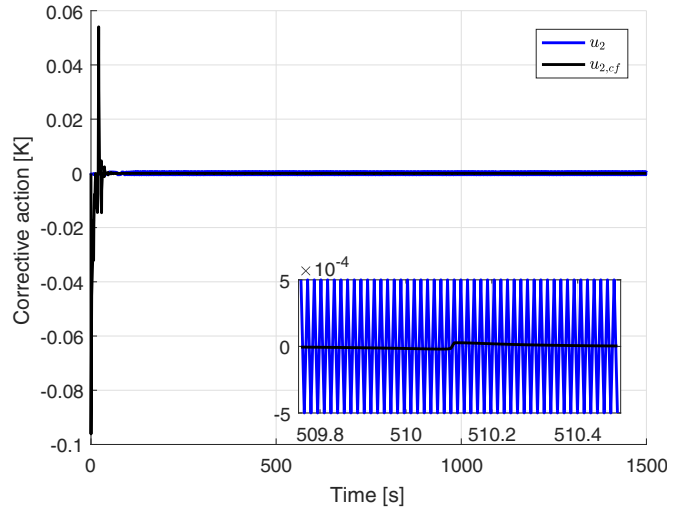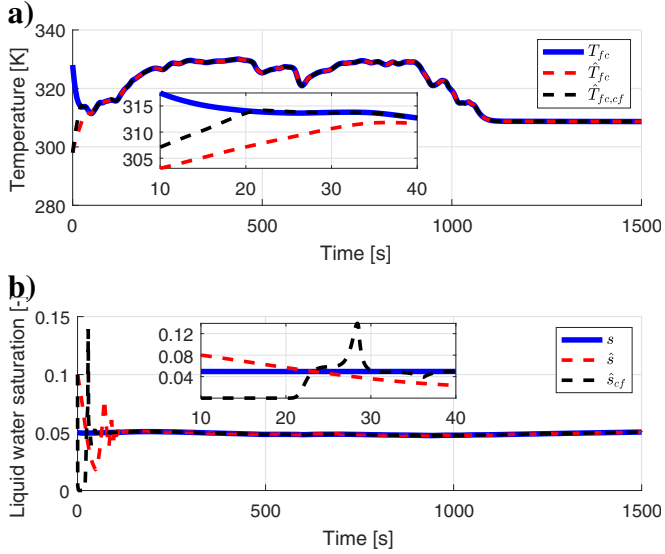

Fig. 5. Temperature (a) and liquid water fraction (b) evolution and observer estimation (HOSM and CHOSM) during the CADC profile

Fig. 6. Evolution of the HOSM and CHOSM corrective actions during the CADC profile

equipment.

The response of the CHOSM corrective action $u_{2,cf}$ has a higher oscillation dynamic before the convergence of the observer with the model states. Nevertheless, it does not have a switching dynamic as shown in the detail of Figure 6. When the observer needs to correct the possible observation error, a small change on the value of $\hat{\beta}$ is enough to drive it back to the sliding surface. This improvement and the faster convergence time shown in Figure 5 corroborates the superior observation capabilities of the CHOSM approach.

VI. CONCLUSIONS

In this paper, a nonlinear CHOSM observer to estimate the liquid water fraction in the cathode side of a PEMFC has been presented. The estimation of this unmeasurable parameter is critical to characterise the PEMFC health state.

Currently, the observation strategy is being implemented in the PEMFC experimental bench presented in Section II in order to experimentally validate the results. After validation, the observer will be used to deploy advanced control solutions to enhance the PEMFC performance and durability.

APPENDIX

A. Model parameters

$$K_1 = \frac{E_{th}n_{cell}}{m_{fc}C_{p,fc}} \tag{22}$$

$$K'_1 = \frac{1}{m_{fc}C_{p,fc}} \tag{23}$$

$$K_2 = \frac{\rho_{air}A_{inlet}C_{p,air}}{m_{fc}C_{p,fc}} \tag{24}$$

$$K_3 = \frac{M_{H_2O}}{2FA_{geo}\epsilon_{eff}d_{CL}\rho_l K_{sorp}} \tag{25}$$

$$K_4 = \frac{K_{evap}M_{H_2O}}{RA_{pore}\epsilon_{eff}d_{CL}\rho_l K_{sorp}} \tag{26}$$

$$K_5 = \frac{n_{cell}R}{\alpha nF} \tag{27}$$

$$K_6 = n_{cell}R_{ohm} \tag{28}$$

$$K_7 = n_{cell}E_0 \tag{29}$$

$$f_a(T_{fc}, s, I_{fc}) = ln\left(\frac{I_{fc}}{A_{geo}i_0^{AECD}}\right) \tag{30}$$

$$f_d(s) = -\frac{J_{diff}}{\epsilon_{eff}d_{CL}\rho_l K_{sorp}} \tag{31}$$

$$f_p(T_{fc}) = \frac{1}{T_{fc}}\left[p^0 \exp\left(\frac{-E_a}{k_B T_{fc}}\right) - p^v\right] \tag{32}$$

ACKNOWLEDGMENT

TABLE I

VALUES OF THE MAIN FUEL CELL PARAMETERS AND PHYSICAL CONSTANTS

Parameter	Value	Units
Specific heat capacity of the fuel cell stack, $C_{p,fc}$	1200	$J \cdot kg^{-1} K^{-1}$
Fuel cell stack mass, m_{fc}	0.3	kg
Air density @ 20^oC, ρ_{air}	1.205	$kg \cdot m^{-3}$
Specific heat capacity of air @ 20^oC, $C_{p,air}$	1005	$J \cdot kg^{-1} \cdot K^{-1}$
Effective cross-section of the cathode housing structure, A_{inlet}	$8.5e^{-3}$	m^2
Theoretical potential @ $T^{ref} = 25^oC$ and $P^{ref} = 1atm$, E_{th}	1.23	V
Number of cells in the stack, n_{cell}	370	$-$
Intrinsic exchange current density of Pt, i_0^{ref}	$5e^{-3}$	$A \cdot m^{-2}$
Charge transfer coefficient, α	0.28	$-$
Activation barrier for the ORR on Pt, ΔG^*	70000	$J \cdot mol^{-1}$
Optimal reachable liquid water saturation, s^{opt}	0.165	$-$
Geometric catalyst surface area, A_{geo}	$22.5e^{-4}$	m^2
Ohmic stack resistance, R_{ohm}	0.7	Ω
Partial pressure of oxygen at the cathode, p_{O_2}	$0.21 \cdot p^{ref}$	Pa
Effective porosity, ϵ_{eff}	0.5	$-$
Effective permeability, K_{eff}	$1e^{-14}$	m^2
Liquid water density, ρ_l	970	$kg \cdot m^{-3}$
Liquid water viscosity, μ_l	$3.517e^{-4}$	$Pa \cdot s$
Liquid water surface tension, σ	0.0625	$N \cdot m^{-1}$
Effective contact angle, θ	91	^{o}
Effective thickness of diffusion media, d_{diff}	$0.41e^{-3}$	m
Catalyst layer volume, V_{CL}	$2.25e^{-8}$	m^3
Catalyst layer thickness, d_{CL}	$0.01e^{-3}$	m
Sorption time constant, K_{sorp}	360	$-$
Evaporation time constant, K_{evap}	$8.6e^5$	$-$
Pre-exponential factor, p^0	$1.196e^{11}$	Pa
Activation energy of evaporation, E_a	0.449	eV
Boltzmann constant, k_B	$8.617e^{-5}$	$eV \cdot K^{-1}$
Cathode ambient pressure, P_{amb}	$1.013e^5$	Pa
Cathode ambient temperature, T_{amb}	298	K
Cathode ambient vapour pressure @ 75% RH, p^v	2380	Pa
Pore surface area per unit volume, A_{pore}	$2e^7$	$m^2 \cdot m^{-3}$

REFERENCES

[1] B. J. De Vries, D. P. Van Vuuren, and M. M. Hoogwijk, "Renewable energy sources: Their global potential for the first-half of the 21st century at a global level: An integrated approach," *Energy Policy*, vol. 35, no. 4, pp. pp. 2590–2610, 2007.

[2] G. Resch, A. Held, T. Faber, C. Panzer, F. Toro, and R. Haas, "Potentials and prospects for renewable energies at global scale," *Energy Policy*, vol. 36, no. 11, pp. pp. 4048–4056, 2008.

[3] B. E. Logan, "Peer reviewed: extracting hydrogen and electricity from renewable resources," *Environmental Science & Technology*, vol. 38, no. 9, pp. pp. 160A–167A, 2004.

[4] S. H. Jensen, P. H. Larsen, and M. Mogensen, "Hydrogen and synthetic fuel production from renewable energy sources," *International Journal of Hydrogen Energy*, vol. 32, no. 15, pp. 3253–3257, 2007.

[5] O. Z. Sharaf and M. F. Orhan, "An overview of fuel cell technology: Fundamentals and applications," *Renewable and Sustainable Energy Reviews*, vol. 32, pp. 810–853, 2014.

[6] J. Luna, E. Usai, A. Husar, and M. Serra, "Nonlinear observation in fuel cell systems: A comparison between disturbance estimation and high-order sliding-mode techniques," *International Journal of Hydrogen Energy*, vol. 41 (43), pp. 19 737–19 748, 2016.

[7] R. Petrone, Z. Zheng, D. Hissel, M.-C. Péra, C. Pianese, M. Sorrentino, M. Becherif, and N. Yousfi-Steiner, "A review on model-based diagnosis methodologies for PEMFCs," *International Journal of Hydrogen Energy*, vol. 38, no. 17, pp. 7077–7091, 2013.

[8] M. Bavarian, M. Soroush, I. Kevrekidis, and J. Benziger, "Mathematical modeling, steady-state and dynamic behavior, and control of fuel cells: A review," *Industrial & Engineering Chemistry Research*, vol. 49, no. 17, pp. pp. 7922–7950, 2010.

[9] N. Yousfi-Steiner, P. Moçotéguy, D. Candusso, D. Hissel, A. Hernandez, and A. Aslanides, "A review on PEM voltage degradation associated with water management: Impacts, influent factors and characterization," *Journal of Power Sources*, vol. 183, no. 1, pp. 260–274, 2008.

[10] D. A. Aligia, G. A. Magallan, and C. H. De Angelo, "Traction control of an electric vehicle based on nonlinear observers," *Revista Iberoamericana de Automática e Informática Industrial*, vol. 15, no. 1, pp. 112–123, 2018.

[11] W. He, G. Lin, and T. Van Nguyen, "Diagnostic tool to detect electrode flooding in proton-exchange-membrane fuel cells," *AIChE Journal*, vol. 49, no. 12, pp. pp. 3221–3228, 2003.

[12] S. Strahl, A. Husar, P. Puleston, and J. Riera, "Performance improvement by temperature control of an open-cathode pem fuel cell system," *Fuel Cells*, pp. 1–3, 2014.

[13] J. Davila, L. Fridman, A. Pisano, and E. Usai, "Finite-time state observation for non-linear uncertain systems via higher-order sliding modes," *International Journal of Control*, vol. 82, no. 8, pp. pp. 1564–1574, 2009.

[14] J.-J. E. Slotine, W. Li, *et al.*, *Applied nonlinear control*. Prentice-Hall Englewood Cliffs, NJ, 1991, vol. 199, no. 1.

[15] A. Levant, "Higher-order sliding modes, differentiation and output-feedback control," *International Journal of Control*, vol. 76, no. 9-10, pp. pp. 924–941, 2003.

[16] S. Mondal and C. Mahanta, "Chattering free adaptive multivariable sliding mode controller for systems with matched and mismatched uncertainty," *ISA transactions*, vol. 52, no. 3, pp. 335–341, 2013.

[17] M. André, "The artemis european driving cycles for measuring car pollutant emissions," *Science of the total Environment*, vol. 334, pp. 73–84, 2004.

[18] "Toyota Mirai," http://www.toyota.com/mirai/fcv.html.

[19] M. Mayur, S. Strahl, A. Husar, and W. G. Bessler, "A multi-timescale modeling methodology for PEMFC performance and durability in a virtual fuel cell car," *International Journal of Hydrogen Energy*, vol. 40, no. 46, pp. pp. 16 466–16 476, 2015.